Phase transitions in high-T_c superconductors and the anisotropic three-dimensional XY model

Tao Chen and S. Teitel
Department of Physics and Astronomy, University of Rochester, Rochester, New York 14627
(Received 18 October 1996)

We carry out simulations of the anisotropic uniformly frustrated three-dimensional XY model, as a model for vortex line fluctuations in high-T_c superconductors. We compute the phase diagram as a function of temperature and anisotropy, for a fixed applied magnetic field B. We find that superconducting coherence parallel to B persists into the vortex line liquid state, vanishing at a T_{cz} above the melting T_m. Both T_{cz} and T_m are found in general to lie well below the crossover T_{c2} from the vortex line liquid to the normal state. [S0163-1829(97)12117-8]

I. INTRODUCTION

From a phenomenological point of view, ''high-T_c'' superconductors are believed to differ from conventional type-II superconductors primarily because of the dramatically enhanced importance of thermal fluctuations.[1–3] In an applied magnetic field **H**, such thermal fluctuations are believed to melt the Abrikosov vortex line lattice at a temperature T_m well below the mean field T_{c2} which marks the onset of strong diamagnetism.[4,5] In between T_m and T_{c2} is a new vortex line liquid state. Experimentally, this picture has been supported by the observation that, in high-T_c materials, the onset of reversible diamagnetism occurs at a temperature well above that where resistance vanishes;[6] the separation between these temperatures increases with increasing H. According to this picture, the onset of diamagnetism at T_{c2} is associated with a growth in local superconducting correlations, giving rise on short length scales to a finite superconducting wave function $\psi(\mathbf{r})$ in terms of which vortex lines can be defined. This T_{c2} marks a strong crossover region, rather than a sharp thermodynamic transition. In the resulting vortex line liquid, free diffusion of vortex lines gives rise to ''flux flow'' electrical resistance. The vanishing of resistance only occurs at a lower temperature when the line liquid freezes into a lattice or glass.

To investigate the effect of thermal fluctuations on phase transitions in type-II superconductors, within a numerical simulation, Li and Teitel have previously introduced[7,8] the three-dimensional (3D) uniformly frustrated XY model. Simulations of this model in the isotropic coupling limit, at a low vortex line density, gave the surprising result that superconducting coherence parallel to the applied magnetic field appeared to persist above the vortex line lattice melting temperature, into the vortex line liquid phase.[8] The goal of the present work is to extend these simulations to a model with uniaxial anisotropic couplings, so as to better model the layered structure of the high-T_c materials. We will consider only the case where the applied magnetic field is parallel to the anisotropy axis $\hat{\mathbf{z}}$. We will map out the phase diagram in the anisotropy-temperature plane, looking for the presence of parallel coherence in the vortex liquid phase and dimensional crossover as the anisotropy increases. The rest of this paper is organized as follows. In Sec. II we describe our model, its limits of validity, and the specific parameters of our simulations. In Sec. III we give our numerical results, mapping out the phase diagram, and characterizing the nature of vortex line fluctuations. In Sec. IV we discuss our results and present our conclusions.

II. MODEL

Our model starts from the Ginzburg-Landau (GL) free energy functional for a continuum superconductor. Making the London approximation that the amplitude of the superconducting wave function is constant outside of the normal vortex core, we have

$$\mathcal{H}[\theta,\mathbf{A}]=\int d^3r\left\{\frac{1}{2}\sum_{\mu}\tilde{J}_{\mu}\left|\nabla_{\mu}\theta-\frac{2\pi}{\phi_0}A_{\mu}\right|^2+\frac{1}{8\pi}|\nabla\times\mathbf{A}|^2\right\}, \tag{1}$$

where $\theta(\mathbf{r})$ is the phase angle of the superconducting wave function, and $\mathbf{A}(\mathbf{r})$ is the magnetic vector potential. The first term is the kinetic energy of flowing supercurrents, and the second term is the magnetic field energy. The integral is implicitly to be cut off at the core of a vortex. In the large-κ approximation which we will be making, the decrease in total condensation energy associated with vortex cores is small compared to the kinetic energy term,[1] and so it is ignored in Eq. (1) and henceforth. The couplings $\tilde{J}_{\mu}$ are given by

$$\tilde{J}_{\mu}=\frac{\hbar^2|\psi_0|^2}{m_{\mu}}=\frac{\phi_0^2}{16\pi^3\lambda_{\mu}^2}, \tag{2}$$

where m_{μ} is the anisotropic mass of the superconducting electrons in direction $\hat{\mu}$, $\phi_0=hc/2e$ is the flux quantum, and the amplitude $|\psi_0|$ of the superconducting wave function outside the normal vortex cores is related to the magnetic penetration length λ_{μ} in direction $\hat{\mu}$ by[2] $\lambda_{\mu}^2=m_{\mu}c^2/16\pi e^2|\psi_0|^2$.

Our next approximation, which we discuss further below, will be to ignore spatial variations and fluctuations in the internal magnetic field, taking $\nabla\times\mathbf{A}=B\hat{\mathbf{z}}$ as a uniform constant. The second term in Eq. (1) thus becomes a constant and is henceforth ignored.

Finally, we discretize the kinetic energy term of Eq. (1) to an orthorhombic grid of points, with grid spacings a_μ in direction $\hat{\mu}$, to get[8]

$$\mathcal{H}[\theta_i] = -\sum_{\langle ij \rangle} J_{ij} \cos(\theta_i - \theta_j - A_{ij}), \tag{3}$$

where θ_i is the phase angle of the wave function at site i of the discrete grid, the sum is over nearest-neighbor bonds $\langle ij \rangle$, $A_{ij} = (2\pi/\phi_0)\int_i^j \mathbf{A} \cdot d\ell$ is the integral of the magnetic vector potential across the bond, and $J_{ij} = (a_x a_y a_z / a_\mu^2)\tilde{J}_\mu$ is the coupling for a bond in direction $\hat{\mu}$. We make the standard substituition of cosine for the the quadratic in Eq. (1) so as to preserve the periodicity of $\mathcal{H}$ with respect to 2π rotations of the phase angles θ_i.

We identify the grid spacings a_μ with the short distance cutoff at a vortex core. For a high-T_c superconductor with CuO layers in the xy plane, we therefore take $a_x = a_y = \xi_\perp$ and $a_z = d$, where $\xi_\perp$ is the coherence length within the CuO planes, and d is the spacing between the CuO planes. We then have $J_{ij} = J_z$ or $J_\perp$, where

$$J_\perp = \frac{\phi_0^2 d}{16\pi^3 \lambda_\perp^2}, \quad J_z = \frac{\phi_0^2 \xi_\perp^2}{16\pi^3 \lambda_z^2 d}, \tag{4}$$

and $\lambda_\perp$ and λ_z are the magnetic penetration lengths within and normal to the CuO planes, respectively. We define an anisotropy parameter η as

$$\eta \equiv \sqrt{\frac{J_\perp}{J_z}} = \frac{\lambda_z}{\lambda_\perp} \frac{d}{\xi_\perp}. \tag{5}$$

Note that if the coherence length along $\hat{\mathbf{z}}$ is larger than the interplanar spacing, $\xi_z > d$, then one should replace d by ξ_z in Eqs. (4) and (5) above. In this case, since the GL free energy with anisotropic masses gives[2] $\xi_z/\xi_\perp = \lambda_\perp/\lambda_z$; we have $\eta = 1$ and hence isotropic couplings. This isotropic model we have investigated previously.[8] In the present paper we extend these studies to the anisotropic case $\eta > 1$.

Our approximation of a uniform magnetic field should be valid provided B is so large that the magnetic fields associated with each vortex line strongly overlap, i.e.,

$$a_v = \sqrt{\phi_0/B} \ll \lambda_\perp, \tag{6}$$

where a_v is the spacing between vortex lines. However B should still be small enough that $a_v \gg \xi_\perp$ (so details of the vortex cores are not important). The anisotropy must also be such that

$$d < \lambda_\perp^2/\lambda_z \quad \text{or, equivalently,} \quad \eta < \lambda_\perp/\xi_\perp, \tag{7}$$

so that the Josephson coupling between the planes dominates over the magnetic coupling.[9,10] Formally, our model corresponds to the limit of $\kappa \equiv \lambda_\perp/\xi_\perp \to \infty$, keeping $J_\perp$ constant. For our simulations, we take the A_{ij} as fixed constants, chosen to give a particular fractional density,

$$f \equiv B\xi_\perp^2/\phi_0, \tag{8}$$

of vortex lines penetrating the xy plane.

Using the model of Eq. (3), which is in terms of the phase angles θ_i, we will also study vortex line fluctuations. To locate a vortex line, we compute the phase angle difference $[\theta_i - \theta_j - A_{ij}]$ across each bond, restricting this angle to the interval $(-\pi, \pi]$. The circulation of these angle differences around any plaquette α must then be $2\pi(n_\alpha - f_\alpha)$, where $f_\alpha = 0$ or f depending on the orientation of the plaquette, and a nonzero integer value of n_α indicates the presence of a vortex line piercing the plaquette. Computing the vorticity of each plaquette in this fashion, we can then trace out the paths of the vortex lines.

To model a particular material, we would like to map out the phase diagram as a function of T and magnetic field B, for a fixed value of anisotropy η. However, due to commensurability difficulties between the triangular vortex lattice preferred in a continuum and the discrete sites permitted by our numerical grid, different vortex line densities would form lattice structures of differing symmetry in the ground state. Since we are computationally limited to a fairly coarse grid, this would make direct comparison of systems with different B difficult. We therefore choose to map out the phase diagram as a function of T and anisotropy η, for fixed B. We can see, however, using dimensional arguments, that increasing η at fixed B is similar to increasing B at fixed η. If we measure any transition temperature T_c in units of $J_\perp$, then the dimensionless $T_c/J_\perp$ can only depend on the other dimensionless parameters of the Hamiltonian (3), the anisotropy $\eta = \lambda_z d/\lambda_\perp \xi_\perp$, and the vortex line density $f = B\xi_\perp^2/\phi_0 = (\xi_\perp/a_v)^2$. Since our London approximation ignores details of the vortex cores, if we consider the continuum limit of our model, $a_v \gg \xi_\perp$, we expect that $T_c/J_\perp$ should be at most weakly dependent[11] on the vortex core radius $\xi_\perp$. The only combination of η and f that is independent of $\xi_\perp$ is $\eta^2 f$. Thus, the dominant dependence of $T_c/J_\perp$ on η and f can only be through some function of $\eta^2 f \sim \eta^2 B$.

We can further argue how transition temperatures should depend on the quantity $\eta^2 f$. In the limit of extreme anisotropy, $\eta \to \infty$, we have completely decoupled planes, and the transition temperature should be independent of η; thus we expect $T_c \sim J_\perp$. In the limit of a nearly isotropic system, $\eta \sim 1$, we expect that T_c should be independent of the spacing between planes d; thus we expect $T_c \sim J_\perp/\eta\sqrt{f} = (\phi_0^2/16\pi^3\lambda_\perp^2)(\lambda_\perp/\lambda_z)(\phi_0/B)^{1/2}$. These are in fact the predictions for the melting temperature based on Lindemann criterion calculations.[2,4,5]

The crossover from small to large η, where the discreteness of the layering along $\hat{\mathbf{z}}$ becomes important and one approaches the two-dimensional limit, can be estimated by the criterion $\eta_{cr}^2 f \simeq 1$ or, using $f = B\xi_\perp^2/\phi_0 = (\xi_\perp/a_v)^2$, as

$$\eta_{cr} = a_v/\xi_\perp. \tag{9}$$

Using an effective elastic medium approximation to describe vortex line fluctuations in the line lattice, one can show[2,9] that for $\eta < \eta_{cr}$, the dominant wave number q_z of fluctuations at melting satisfies the condition $d < \pi/q_z$, and hence the layering of the material is averaged over. For

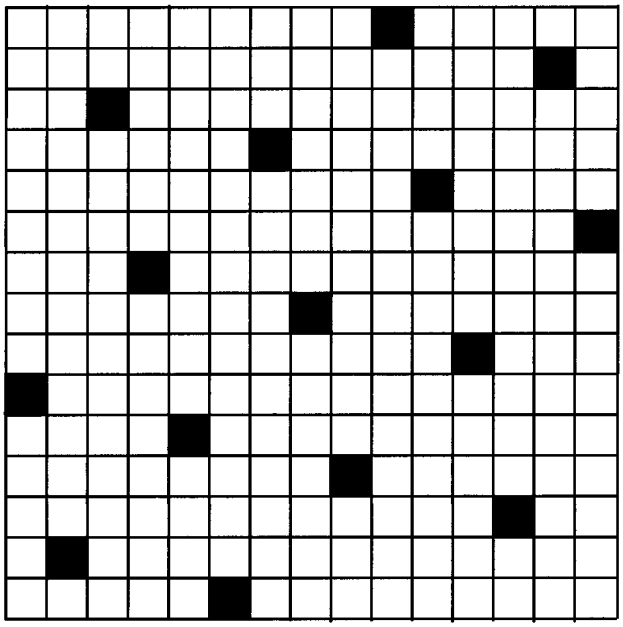

FIG. 1. Ground-state locations of vortex lines in the xy plane for line density $f=1/15$ on a cubic grid.

$\eta > \eta_{\rm cr}$, however, the dominant wave number is at $d=\pi/q_z$, and layering is important. Some theoretical models[9,12,13] have predicted that $\eta_{\rm cr}$ (or equivalently $B_{\rm cr}=\phi_0\lambda_\perp^2/\lambda_z^2 d^2$) will mark a dramatic change in behavior, reflecting a three-dimensional to two-dimensional crossover. Looking for any such crossover behavior at $\eta_{\rm cr}$ will be one of the goals of this work.

Our simulations consist of standard Metropolis Monte Carlo simulations of the Hamiltonian (3), using periodic boundary conditions in all directions, on grid sizes $L_\perp^2 \times L_z$. We use a magnetic field B which yields a fractional density of vortex lines $f=1/15$. The ground state vortex lattice, shown in Fig. 1, is a nearly triangular vortex line lattice with sides of length $\sqrt{18}\times\sqrt{18}\times\sqrt{17}$ in units of $\xi_\perp$. To map out the η-T phase diagram, we have done simulations varying T at different fixed values of η on lattices of size 15^3. We have also carried out simulations of larger system sizes for the specific cases of $\eta^2=10<\eta_{\rm cr}^2=1/f=15$ and $\eta^2=50>\eta_{\rm cr}^2$. Our runs are typically 10 000 sweeps through the grid to equilibrate, followed by 128 000 sweeps to compute averages. These simulations are about 9 times longer than in our previous work.[8] Errors are estimated by a standard data-blocking procedure.

III. NUMERICAL RESULTS

A. Phase diagram

To test for superconducting coherence, we compute the helicity moduli $\Upsilon_\perp(T)$ and $\Upsilon_z(T)$ which measure the stiffness with respect to applying a net gradient (''twist'') in the phase angle of the wave function along directions perpendicular and parallel to the applied magnetic field.[8] The helicity modulus in direction $\hat{\mu}$ is given by the phase angle correlation

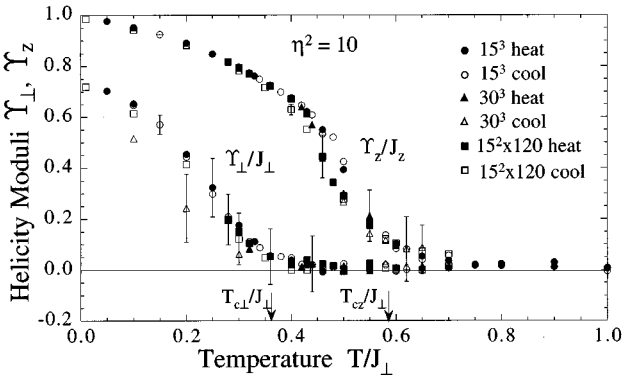

FIG. 2. Helicity moduli $\Upsilon_\perp$ and Υ_z vs temperature T for anisotropy $\eta^2=10$ and vortex line density $f=1/15$. Heating and cooling data for three different system sizes are shown, along with representative errors.

$$\Upsilon_\mu(T)=\frac{1}{L_\perp^2 L_z}\left\langle \sum_{\langle ij\rangle} J_{ij}\cos(\theta_i-\theta_j-A_{ij})(\hat{\mathbf{e}}_{ij}\cdot\hat{\mu})^2\right\rangle - \frac{1}{TL_\perp^2 L_z}\left\langle\left[\sum_{\langle ij\rangle} J_{ij}\sin(\theta_i-\theta_j-A_{ij})(\hat{\mathbf{e}}_{ij}\cdot\hat{\mu})\right]^2\right\rangle, \tag{10}$$

where $\hat{\mathbf{e}}_{ij}$ is the unit vector from site i to j. When Υ_μ is positive, the system can carry a supercurrent, and so possesses superconducting coherence in direction $\hat{\mu}$. When Υ_μ vanishes, superconducting coherence is lost.

To determine the vortex line lattice melting temperature, we compute the density-density correlation function of vortices within the same plane,

$$S(\mathbf{k}_\perp)=\frac{1}{L_z}\sum_{\mathbf{r}_\perp,\mathbf{r}'_\perp,z} e^{i\mathbf{k}_\perp\cdot(\mathbf{r}_\perp-\mathbf{r}'_\perp)}\langle n_z(\mathbf{r}_\perp,z)n_z(\mathbf{r}'_\perp,z)\rangle, \tag{11}$$

where $n_z(\mathbf{r}_\perp,z)$ is the vorticity at site $\mathbf{r}_\perp$ in the xy plane at height z (henceforth, we will refer to the vortices in the xy planes as the ''pancake'' vortices). Below melting, we expect to see a periodic array of sharp Bragg peaks in the $\mathbf{k}_\perp$ plane. Above melting, we expect to see the broad circular rings characteristic of a liquid.

We also compute the specific heat per site of the system, C, using the usual energy fluctuation formula. A peak in C locates the temperature at which, upon cooling, there is a dramatic freezing out of thermal fluctuations and the system loses the bulk of its entropy. We will take the location of a high-temperature peak (above any phase transitions) in C as indicating the crossover temperature T_{c2} where the superconducting wave function develops on small length scales, vortex lines become well-defined objects, and one has the onset of strong diamagnetism.

In Fig. 2 we show our results for $\Upsilon_\perp$ and Υ_z for the case $\eta^2=10$. We see that $\Upsilon_\perp$ vanishes at a $T_{c\perp}$ significantly lower than the T_{cz} where Υ_z vanishes. We show data for heating and cooling, for three different grid sizes 15^3, 30^3, and $15^2\times 120$. Comparing heating and cooling, we see no appreciable hysteresis for Υ_z. Hysteresis in $\Upsilon_\perp$ appears only for the 30^3 system, where we failed to cool back into a lattice.

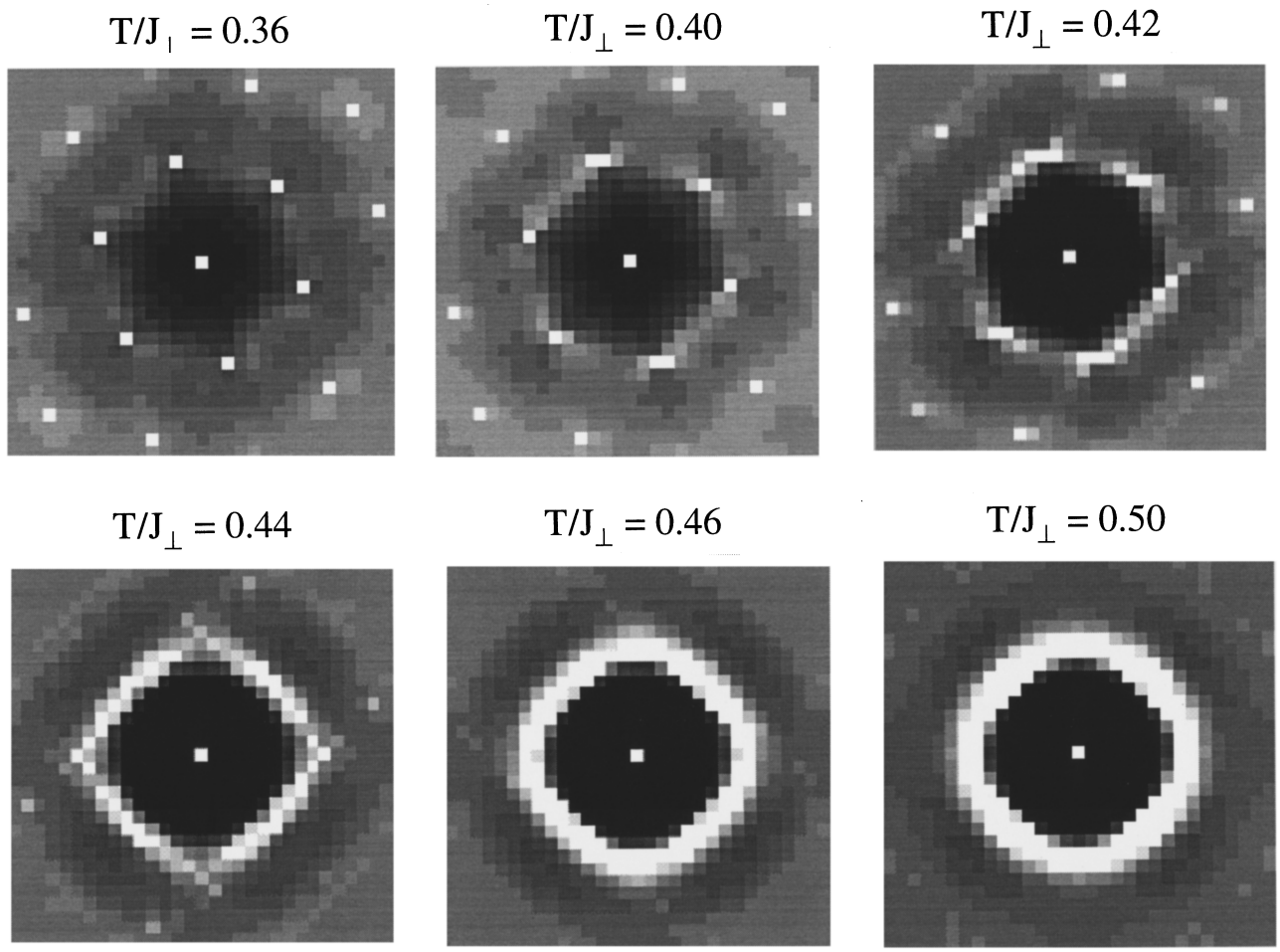

FIG. 3. Structure function $S(\mathbf{k}_\perp)$ for $\eta^2=10$ and $f=1/15$ for system size 30^3, upon heating. The crossover from Bragg peaks to liquidlike rings occurs at $T_m/J_\perp \simeq 0.43$.

There are no obvious shifts in T_{cz} or $T_{c\perp}$ due to finite-size effects as $L_\perp$ and L_z are varied. We determine our estimates $T_{c\perp}/J_\perp \simeq 0.36$ and $T_{cz}/J_\perp \simeq 0.58$ by visually extrapolating the curves to zero from the inflection point that marks the onset of the high-temperature tails. We have found that the size of these tails tends to decrease with increasing simulation time, as well as with system size.

It is important to note that the finite $T_{c\perp}$ in our model is strictly an artifact of the discretizing grid, which acts like an effective periodic pinning potential for the vortex lines. In a continuum model, one would find $\Upsilon_\perp=0$ at *all* temperatures,[14] as the vortex line lattice is free to slide as a whole, giving ''flux flow resistance.'' A discretizing grid removes this translational symmetry, resulting in a commensurately pinned vortex line lattice at low temperatures, with $\Upsilon_\perp>0$. For a high density of vortex lines, it is likely that the vortex lattice remains commensurately pinned until it melts. In such a case one expects $T_m=T_{c\perp}$. However, recent simulations,[15–17] with a more dilute vortex line density than studied here, have claimed evidence for a depinning $T_{c\perp}$ which is lower than T_m, with the intermediate phase a floating vortex line lattice. It is thus important to determine the melting T_m of our vortex lattice independently from our measurement of $\Upsilon_\perp$.

In Fig. 3 we show intensity plots at various temperatures of $S(\mathbf{k}_\perp)$ in the $\mathbf{k}_\perp$ plane, for the 30^3 system upon heating. Looking at when the Bragg peaks disappear, we estimate the melting temperature to be $T/J_\perp \simeq 0.43$, somewhat higher than $T_{c\perp}/J_\perp \simeq 0.36$. To try to quantify the location of the melting transition, we now look at the heights of the Bragg peaks at the reciprocal lattice vectors. We denote by $\{\mathbf{K}_1\}$ the six, almost equal, smallest nonzero reciprocal lattice vectors. Let $\{\mathbf{K}_1'\}$ be the six vectors obtained by reflecting the $\{\mathbf{K}_1\}$ through the $\hat{\mathbf{x}}$ axis. Since the vortex line lattice breaks this reflection symmetry of the square discretizing grid, we will have $S(\mathbf{K}_1)>S(\mathbf{K}_1')$ for the lattice phase. However, once the lattice has melted, the reflection symmetry of the grid should be restored. We can therefore define as an order parameter of the melting transition $\Delta S(\mathbf{K}_1)\equiv S(\mathbf{K}_1)-S(\mathbf{K}_1')$. Normalizing by $S_0\equiv S(\mathbf{K}=0)$ and averaging over the six $\{\mathbf{K}_1\}$, we plot, in Fig. 4, $\Delta S(\mathbf{K}_1)/S_0$ versus T, for the three system sizes 15^3, 30^3, and $15^2\times 120$. $\Delta S(\mathbf{K}_1)/S_0$ decreases linearly over a large intermediate range of T. From the 30^3 system we estimate $T_m/J_\perp \simeq 0.44$. Note that there is a greater finite-size effect and more hysteresis for $\Delta S(\mathbf{K}_1)/S_0$ than there is in $\Upsilon_{\perp,z}$. The estimate for T_m tends to decrease as $L_\perp$ increases. Our result $T_{c\perp}<T_m$ suggests the presence of a floating vortex line lattice. However, it remains possible that $T_{c\perp}$ and T_m will merge as the system size increases, due

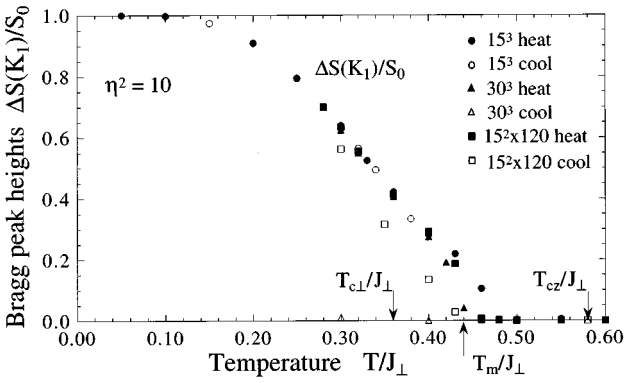

FIG. 4. Bragg peak heights $\Delta S(\mathbf{K}_1)/S_0$ for $\eta^2=10$, $f=1/15$, and different system sizes.

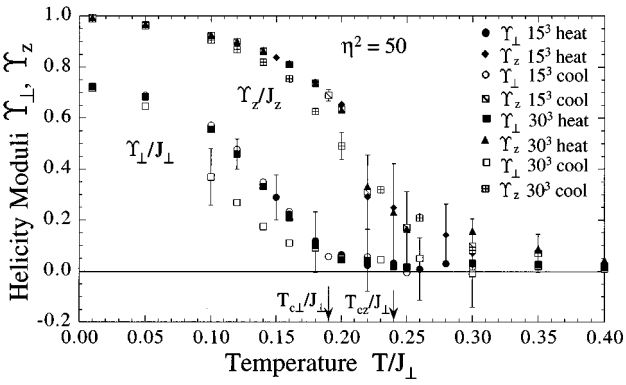

FIG. 6. Helicity moduli $\Upsilon_\perp$ and Υ_z vs temperature T for anisotropy $\eta^2=50$ and vortex line density $f=1/15$. Heating and cooling for two different system sizes are shown, along with representative error bars.

either to the finite-size dependence observed in $T_{\rm m}$ or to the possibility that $T_{c\perp}$ actually lies farther out in the high-temperature tail of $\Upsilon_\perp$ than we have estimated.

Finally, in Fig. 5 we show the specific heat C. The high-temperature peak in C at $T/J_\perp \simeq 1.0$ we identify with the crossover T_{c2}, which is thus seen to lie well above $T_{c\perp}$, $T_{\rm m}$, and T_{cz}. A suggestion of a smaller peak is seen at the lower temperature $T_{c\perp}$.

In Fig. 6 we show $\Upsilon_\perp$ and Υ_z for the case $\eta^2=50$, for system sizes 15^3 and 30^3. Here the data have considerably more scatter than in Fig. 2 (in general, we found it increasingly difficult to achieve good equilibration as η increased). Nevertheless, there again appears to be two distinct transitions, with $T_{c\perp}/J_\perp \simeq 0.19 < T_{cz}/J_\perp \simeq 0.24$. Intensity plots of the structure function $S(\mathbf{k}_\perp)$ are shown in Fig. 7 and the peak height differences $\Delta S(\mathbf{K}_1)/S_0$ in Fig. 8. These suggest a melting $T_{\rm m}/J_\perp \simeq 0.21$. In Fig. 9 we show the specific heat C. The high-temperature peak at $T/J_\perp \simeq 1.0$ is again associated with T_{c2}. However, comparing with Fig. 5, there is now a more clearly defined smaller peak at $T_{c\perp}$.

Carrying out simulations at other values of η on a 15^3 grid, we show in Fig. 10 the resulting phase diagram in the η-T plane. The T_{cz} line denotes the loss of phase coherence parallel to the applied magnetic field, as measured by the vanishing of Υ_z. The $T_{\rm m}$ line denotes the melting of the vortex line lattice, as measured by the vanishing of $\Delta S(\mathbf{K}_1)/S_0$. The $T_{c\perp}$ line denotes the depinning of the vortex line lattice from the discretizing grid, as measured by the vanishing of $\Upsilon_\perp$. We see that $T_{\rm m}$ coincides with $T_{c\perp}$ in the $\eta \sim 1$ and $\eta \gg \eta_{\rm cr}$ limits, but is somewhat greater than $T_{c\perp}$ in the vicinity of the crossover anisotropy $\eta_{\rm cr}=a_{\rm v}/\xi_\perp=\sqrt{15}$. Between $T_{\rm m}$ and T_{cz} we have a vortex line liquid which retains superconducting coherence in the direction parallel to the applied magnetic field. The dashed line T_{c2} locates the high-temperature peak of the specific heat and marks the crossover from the the vortex line liquid to the normal metal. The dotted lines labeled $\xi_c=n$ will be explained at the end of the following section.

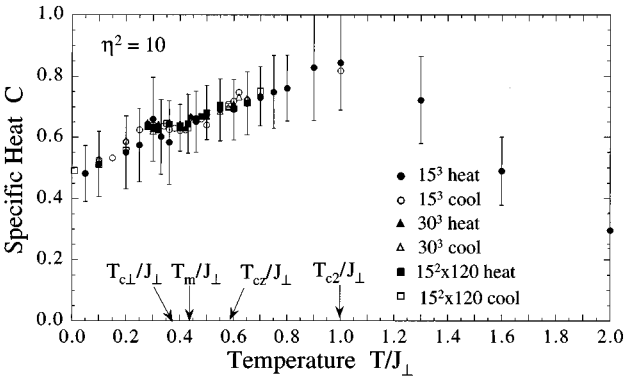

FIG. 5. Specific heat C vs T for $\eta^2=10$, $f=1/15$, and various system sizes. The high-temperature peak locates the crossover T_{c2}.

Thus, for $T_{c2}<T$ we have the resistive normal metal with weak diamagnetism. For $T_{cz}<T<T_{c2}$ we have a vortex line liquid, with strong diamagnetism but still with resistive behavior in all directions. For $T_{\rm m}<T<T_{cz}$ we have a vortex line liquid with superconducting coherence parallel to **B**. For $T<T_{\rm m}$ we have an Abrikosov vortex line lattice. For $T<T_{c\perp}$ the vortex line lattice is pinned.

If we fit the lowest five data points (those for $\eta \leqslant \eta_{cr}$) to a power law, we find $T_{c\perp} \sim \eta^{-0.88\pm0.09}$, $T_{cz} \sim \eta^{-0.98\pm0.05}$, and $T_{\rm m} \sim \eta^{-0.66\pm0.07}$. The results for $T_{c\perp}$ and T_{cz} are in good agreement with our dimensional argument that characteristic temperatures at small η should scale as $T \sim \eta^{-1}$. The agreement of $T_{\rm m}$ with this form is much poorer. Whether this reflects the inclusion of too large values of η in the fit or whether it reflects a poor determination of $T_{\rm m}$ due to finite-size effects or incomplete equilibration remains unclear. At large η, all three lines approach the constant value $T_{\rm c}^{\rm 2D}$, which we have found from independent simulations to be the melting temperature for an isolated two-dimensional plane.[18]

We see that T_{c2} for $\eta > \eta_{\rm cr}$ becomes independent of η, and is located at the same temperature as the specific heat peak in the ordinary ($B=0$) 2D XY model[19] (which lies about 10% above the 2D XY Kosterlitz-Thouless transition at $T_{\rm KT}/J_\perp \simeq 0.9$). Thus, at these high temperatures, $\eta_{\rm cr}$ does indeed mark the dimensional crossover where our three-dimensional system is behaving as effectively decoupled 2D layers; the crossover T_{c2} is due to the proliferation of vortex-antivortex pairs within these decoupled layers. However, at lower temperatures, we see no dramatic change in the behavior for $T_{c\perp}$, $T_{\rm m}$, and T_{cz} as $\eta_{\rm cr}$ is crossed. Layers remain

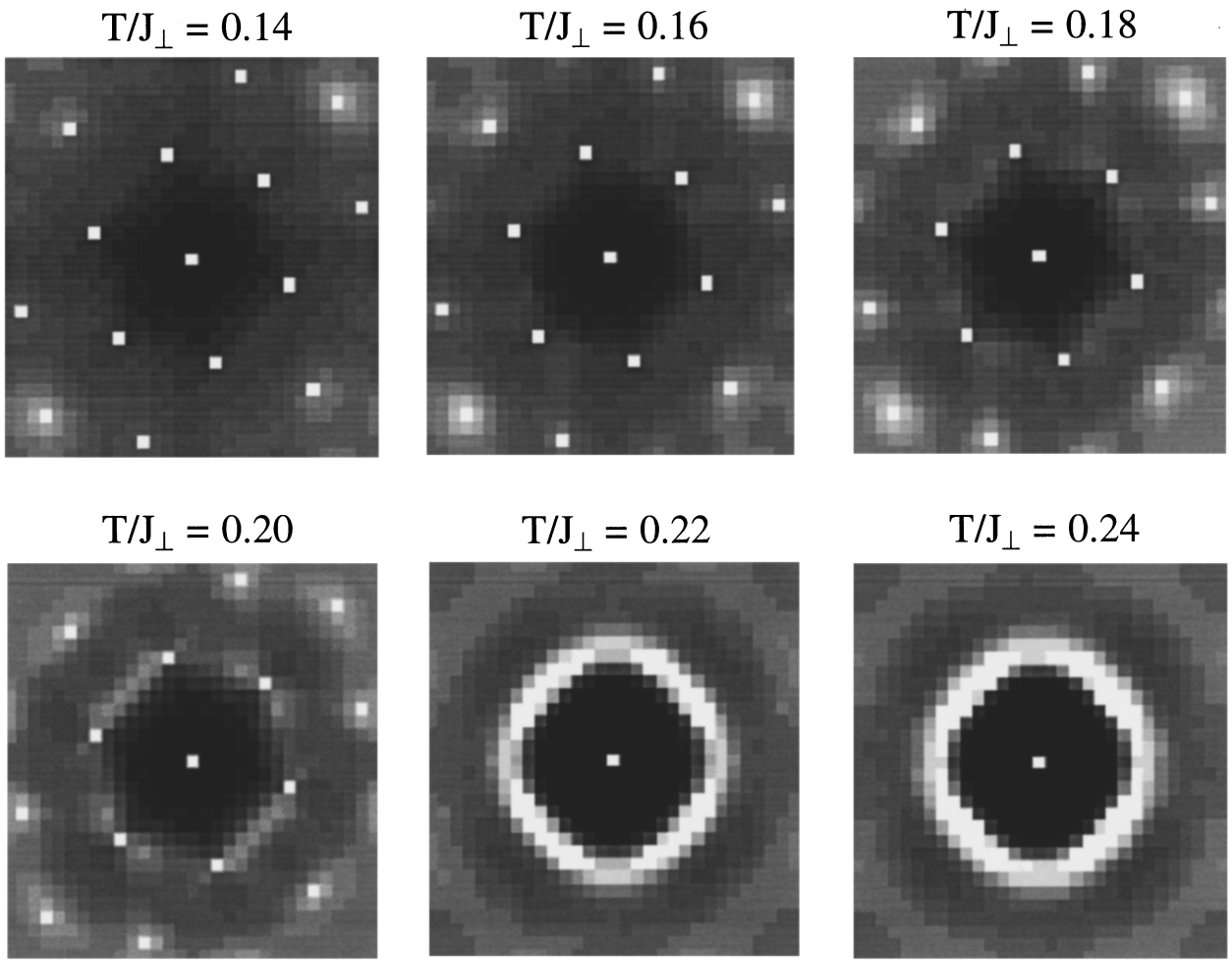

FIG. 7. Structure function $S(\mathbf{k}_\perp)$ for $\eta^2=50$ and $f=1/15$ for system size 30^3, upon heating. The crossover from Bragg peaks to liquidlike rings occurs at $T_m/J_\perp \simeq 0.21$.

coupled, and in particular, while $T_{c\perp}$, T_m, and T_{cz} appear to merge as η increases, we continue to find $T_{c\perp} \leq T_m \leq T_{cz}$ for all $\eta > \eta_{cr}$ studied.

Note that in the limit of weak anisotropy, $\eta \to 1$, T_{cz} and T_{c2} become close, as was observed in earlier isotropic simulations.[8] However, once the anisotropy η increases, T_{cz} falls well below T_{c2}. The transition at T_{cz} is thus clearly distinct from any mean-field-like crossover phenomena. We will discuss this point in greater detail in the following section. Using the analogy between increasing η and increasing B as discussed in Sec. II, the increase in the width of the

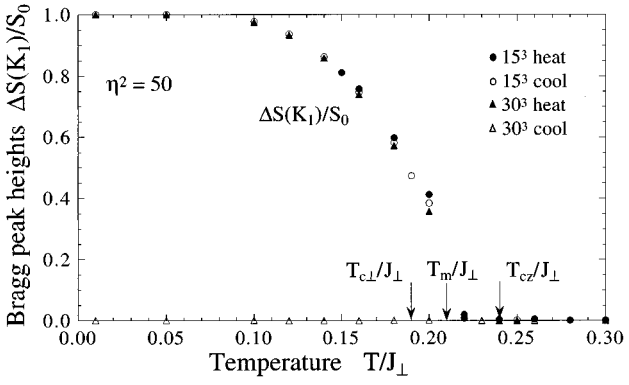

FIG. 8. Bragg peak heights $\Delta S(\mathbf{K}_1)/S_0$ for $\eta^2=50$, $f=1/15$, and different system sizes.

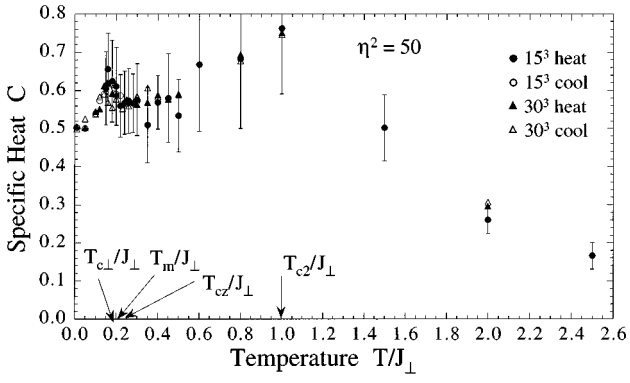

FIG. 9. Specific heat C vs T for $\eta^2=50$, $f=1/15$, and various system sizes. The high-temperature peak locates the crossover T_{c2}. A lower-temperature peak corresponds to $T_{c\perp}$.

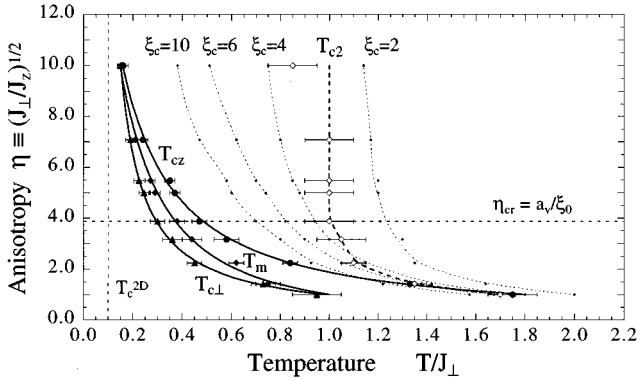

FIG. 10. Phase diagram in the anisotropy-temperature plane for vortex line density $f=1/15$. ξ_c is measured in units of d. T_{c2} locates the peak in specific heat.

vortex line liquid region in Fig. 10, as anisotropy increases, is in agreement with the general experimental features discussed in the Introduction.

B. Vortex line fluctuations

We now discuss several measures of the vortex line fluctuations in our model, in order to try and clarify the nature of the phenomena at T_{cz} and T_{c2}.

The first quantity we consider is $\Delta\ell_\mu$, defined as the the total number of vortex line segments due to fluctuations in direction $\hat{\mu}$, normalized by the total number of field-induced ''pancake'' vortices in the xy planes, $fL_\perp^2 L_z$. Note that in computing $\Delta\ell_\mu$, line segments are added without regard to the sign of their direction; oppositely oriented segments do *not* cancel out. In Figs. 11(a) and 11(b) we show our results for $\Delta\ell_\perp \equiv \frac{1}{2}(\Delta\ell_x + \Delta\ell_y)$ and $\Delta\ell_z$ for the two cases of $\eta^2=10$ and $\eta^2=50$, respectively. We see that in both cases, $\Delta\ell_z$ is at least two orders of magnitude smaller than $\Delta\ell_\perp$ in the vicinity of T_{cz} and below. Thus, only transverse vortex fluctuations appear to be important at the phase transitions. Only at the higher crossover T_{c2} does $\Delta\ell_z$ start to become comparable to $\Delta\ell_\perp$. This is consistent with our interpretation of T_{c2} as the temperature at which vortex-antivortex pairs start to enter the xy planes.

One possible explanation for the transition at T_{cz} has been proposed by Nelson and Seung[4] in terms of the entanglement of vortex lines. If we assume, as in the Nelson-Seung picture, that the transverse fluctuation of a vortex line in the liquid phase is like that of a random walk, then since $\Delta\ell_\perp$ is the net transverse fluctuation per pancake vortex, the total transverse deflection of a line in traveling down the length of the system will be $u=\sqrt{L_z}\Delta\ell_\perp$. Geometric entanglement[20] of lines should occur when $u \simeq a_v$ or when $\Delta\ell_\perp \simeq a_v/\sqrt{L_z} = 1/\sqrt{fL_z}$. For our system with $f=1/15$, this criterion gives entanglement at values of $\Delta\ell_\perp = 1.0$, 0.71, and 0.35 for thicknesses $L_z=15$, 30, and 120, respectively. Noting that $\Delta\ell_\perp$ shows no apparent dependence on L_z near the transitions, we would conclude that geometric entanglement takes place noticeably *below* T_{cz} for systems of thickness $L_z>15$. It is interesting to note that in both cases, Figs. 11(a) and 11(b), T_{cz} appears to coincide with the point where

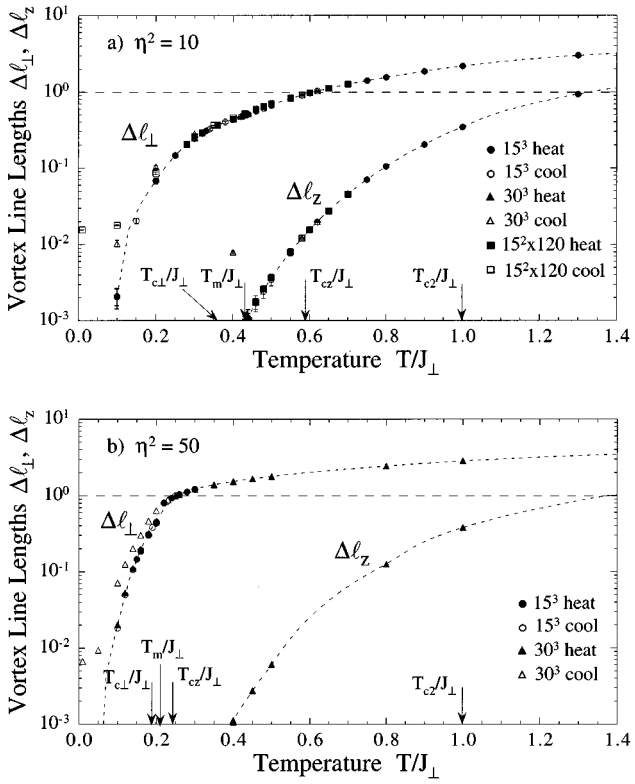

FIG. 11. Excess vortex line length due to fluctuations in transverse, $\Delta\ell_\perp$, and parallel, $\Delta\ell_z$, directions. (a) is for $\eta^2=10$; (b) is for $\eta^2=50$. Dashed lines are guides to the eye only.

$\Delta\ell_\perp \simeq 1$. We have similarly observed this to be true at other values of η. However, we have no explanation for this coincidence.

The above argument assumed that all of the vortex line fluctuations consisted of transverse motions of the magnetic-field-induced vortex lines. However, there is additionally the possibility of forming thermally excited closed vortex rings, which for large enough η and temperatures low compared to T_{c2} should tend to lie between two adjacent xy planes. We now describe our algorithm to trace out the paths of vortex lines, which will allow us to measure both the distribution of such closed rings, as well as the entanglement of the field induced lines. We start by searching the plaquettes for a penetrating vortex line segment. We then trace its path into and out of subsequent unit cells of the grid. Such a line can belong either to a field induced vortex line or to a closed vortex ring. Tracing the line, we measure the net displacement parallel to $\hat{\mathbf{z}}$ that is traveled before the line closes back upon itself. If we have a closed ring, this net displacement is zero, and we measure the perimeter of the ring p. If we have a field induced line, then because of our periodic boundary conditions parallel to $\hat{\mathbf{z}}$, this net displacement must be mL_z with integer $m=1,2,\ldots,fL_\perp^2$. If $m=1$, the line closes back upon itself upon traversing the length of the system L_z. For $m>1$, the line belongs to a group of m lines that are braided with each other. This is schematically illustrated in Fig. 12. The distribution of values of m is a measure of how geometrically entangled the field induced lines are. With this procedure, we search through all plaquettes until all vortex line segments are found and classified as belonging to either

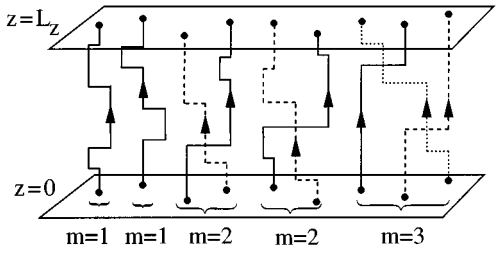

FIG. 12. Schematic example of the possible reconnections of field-induced vortex lines, under application of the periodic boundary condition in the $\hat{\mathbf{z}}$ direction. Solid, dashed, and dotted lines are used to distinguish the different lines within a particular braid.

a ring of perimeter p or an entangled braid of order m. The only complication in the above algorithm occurs when two or more vortex lines segments intersect, i.e., go in and out of the same unit cell of the grid. In this case we randomly choose which segment is connected to which. In practice this was achieved as follows. Once a line was traced into a unit cell, we searched the remaining five faces in a random order to see which face the line is leaving through. Once we find a line leaving, we take it to be the continuation of the line we are tracing.

In Figs. 13(a) and 13(b) we show our results for the distribution $q(p)$ of the number of closed rings of perimeter p per unit volume $L_z L_\perp^2$, for the two cases $\eta^2=10$ and $\eta^2=50$ (we show results for cooling; no significant hysteresis was observed comparing heating and cooling). Plotting the logarithm of $q(p)$ versus $1/T$, we see approximately straight lines at low T, indicating thermal activation. These lines have a change in slope in the vicinity of the melting

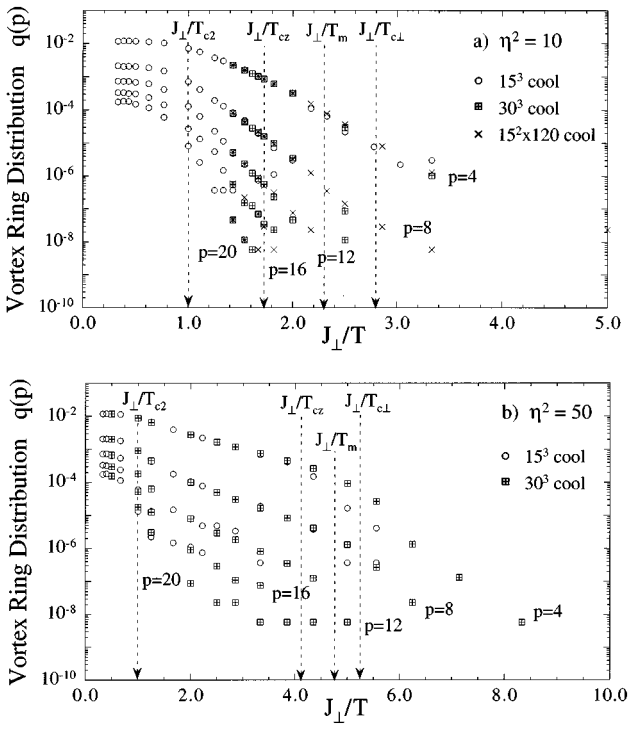

FIG. 13. Number of closed vortex rings $q(p)$ of perimeter p, per unit volume. (a) is for $\eta^2=10$; (b) is for $\eta^2=50$.

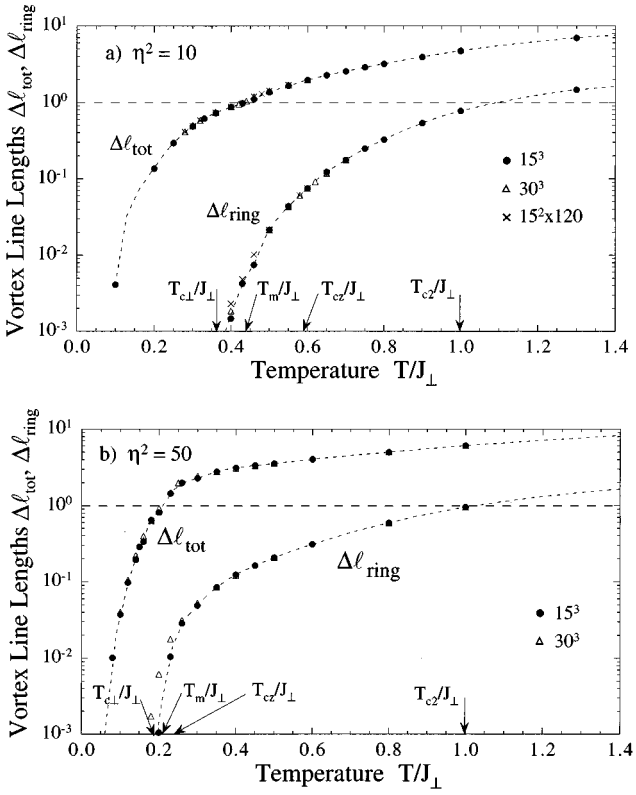

FIG. 14. Total length of all vortex line fluctuations, $\Delta\ell_{\rm tot}$, and total length of lines in closed vortex rings, $\Delta\ell_{\rm ring}$, per number of pancake vortices. (a) is for $\eta^2=10$; (b) is for $\eta^2=50$.

$T_{\rm m}$, which is mild for $\eta^2=10$, but more pronounced for $\eta^2=50$. At the higher T_{c2} the curves saturate. We believe this is consistent with the interpretation of T_{c2} as the crossover temperature at which, upon heating, vorticity explodes throughout the system, and superconducting order is lost on even small length scales. The saturation of $q(p)$ occurs because, above T_{c2}, the distribution of ring sizes is governed more by the statistics of random intersections among the lines, rather than by energetics. Note that in Ref. 8, where only the isotropic case was studied, we incorrectly associated this explosion of vorticity, as indicated by the saturation of $q(p)$, with the transition at T_{cz}. From the phase diagram of Fig. 10, we now see that this mistake was due to the proximity of T_{c2} and T_{cz} which occurs only in the isotropic limit. For anisotropic systems, T_{cz} drops below T_{c2} and lies in the region where $q(p)$ is still governed by thermal activation.

From the data of Figs. 11 and 13, we can now compare how much of the vortex line fluctuations is contained in the wandering of the field-induced vortex lines versus how much is contained in the thermally excited vortex rings. We show in Figs. 14(a) and 14(b) the total length of *all* vortex line fluctuations (per pancake vortex), $\Delta\ell_{\rm tot}\equiv 2\Delta\ell_\perp+\Delta\ell_z$, and the total length contained in closed vortex rings (per pancake vortex), $\Delta\ell_{\rm ring}\equiv f^{-1}\Sigma_p pq(p)$, for the cases $\eta^2=10$ and $\eta^2=50$, respectively. We see that at low temperatures, rings constitute a negligible fraction of the total vortex line fluctuations. At the transition T_{cz} they are only about 3.5% of the fluctuations for $\eta^2=10$ and 1.5% for $\eta^2=50$. It thus seems that as anisotropy increases, the importance of disconnected thermally excited vortex rings decreases. It is worth noting,

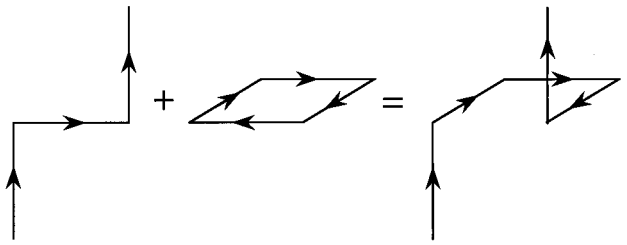

FIG. 15. Schematic example of how ''connected'' vortex rings between planes contribute to the wandering of field-induced lines between planes.

however, that ring excitations which connect to field-induced lines may still play a role in determining the wandering of the magnetic-field-induced lines between planes. An example is illustrated in Fig. 15. Such ''connected'' ring excitations, which lie between xy planes, are degrees of freedom distinct from the pancake vortices, which lie within the planes. In Figs. 16(a) and 16(b), we show snapshot views of vortex line configurations, at various temperatures, for the cases $\eta^2=10$ and $\eta^2=50$, for a system of size 15^3. The bottom row in each figure is a view of all vortex line segments that lie between a typical pair of adjacent xy planes. A ''$\sqcup$'' shaped segment in these bottom row views indicates a connected ring excitation. We see that they are present in the system at virtually all temperatures shown; however, it remains unclear how, if at all, they correlate with the transitions.

We turn now to consider the fluctuations of the magnetic-field-induced vortex lines. As mentioned in connection with our line tracing algorithm, we can classify each such line as belong to an entangled braid of m lines, $m=1,\ldots,fL_\perp^2$ (see Fig. 12). We denote by $n(m)$ the number of lines which participate in a braid of order m, and $R\equiv n(1)/fL_\perp^2$ is the fraction of unentangled lines. In Figs. 17(a) and 17(b) we plot R versus T for the cases $\eta^2=10$ and $\eta^2=50$, respectively. We see that upon heating, $R=1$ up to $T_{\rm m}$, throughout the vortex line lattice phase. Above $T_{\rm m}$, R starts to drop, tending to saturate to its high-T limit around $T_{\rm cz}$. Upon cooling, R starts to increase at $T_{\rm cz}$, and in most cases reaches a completely disentangled configuration with $R=1$ at $T_{\rm m}$. These features were found at all values of η studied. For the thickest sample of $L_z=120$ at $\eta^2=10$, however, we cool into a glassy entangled state with $R\simeq 0.47$ frozen below $T_{\rm c\perp}$, as has been seen in previous isotropic simulations.[8] From Fig. 17 it seems clear that the transition at $T_{\rm cz}$ is related to the braiding of lines.

To see this another way, we plot in Figs. 18(a) and 18(b), for $\eta^2=10$ and $\eta^2=50$, respectively, the braid distribution $n(m)$ versus m, for several different temperatures near $T_{\rm cz}$. We use our data for systems of size 30^3, which have 60 lines. We see that for $T<T_{\rm cz}$, $n(m)$ is strongly peaked at small m, decaying rapidly as m increases. However, as $T_{\rm cz}$ is approached, the peak at small m decreases and the distribution $n(m)$ becomes flat and equal to unity for an increasingly wide range of intermediate m. The transition at $T_{\rm cz}$ therefore seems to be associated with braids involving a macroscopically large number of lines. When $n(m)=1$ for *all* m, it indicates that a line i which starts out at $\mathbf{r}_{i\perp}(z=0)$ in the xy plane at $z=0$ is equally likely to match onto the starting position of any other line j, after traveling down the thickness of the system; i.e., $\mathbf{r}_{i\perp}(z=L_z)=\mathbf{r}_{j\perp}(z=0)$ is equally likely for any pair i and j (see Fig. 12). We may speculate that precisely this condition is achieved at $T_{\rm cz}$ in the limit of large system sizes and long simulation times.

An intriguing question concerning behavior in the vortex line liquid is how easily lines can cut through each other. This has important consequences for line diffusion. If lines cannot cut, they can be effectively pinned by their mutual entanglements.[4,21] For our system in particular, with periodic boundary conditions parallel to the magnetic field, the degree of entanglement can only change due to the cutting and reconnecting of lines. To investigate this we have computed the average number of vortex line intersections, $N_{\rm c}$, present in any instantaneous configuration of the system. An intersection is defined when two vortex lines enter and leave the same unit cell of the grid, and corresponds to vortex lines with overlapping cores. Once two lines intersect, they are free to cut through each other or even to detach and reconnect different ingoing and outgoing segments. We define the ''cutting length'' $\xi_{\rm c}\equiv fL_\perp^2 L_z/N_{\rm c}$ as the average distance (in units of d) along $\hat{\mathbf{z}}$ between cuts of the magnetic-field-induced vortex lines. $\xi_{\rm c}$ gives a crude measure of the average length over which a vortex line remains a well-defined string or equivalently, a measure of the number of planes which remain correlated. In Fig. 19 we plot $\xi_{\rm c}$ versus T for the two cases $\eta^2=10$ and $\eta^2=50$. In the phase diagram of Fig. 10 we show contours of constant $\xi_{\rm c}=2$, 4, 6, and 10. We see that planes are essentially uncorrelated at temperatures above the crossover $T_{\rm c2}$. However, correlations grow and get large as one cools below $T_{\rm c2}$ towards $T_{\rm cz}$. The picture presented by the contours of $\xi_{\rm c}$ in Fig. 10, combined with the behavior of R in Fig. 17 and $n(m)$ in Fig. 18, is that intersections start to freeze out below $T_{\rm c2}$, with lines becoming well defined on longer and longer length scales. This presumably will affect the time scales on which lines are able to diffuse about, with a corresponding signature to be expected in dynamic phenomena. However, the equilibrium degree of entanglement, as measured by R and $n(m)$, remains largely unchanged down to $T_{\rm cz}$. Below $T_{\rm cz}$, the behavior of R and $n(m)$ shows that the lines start to disentangle, yet cutting is still frequent enough to change the degree of entanglement for all temperatures down to $T_{\rm m}$. Below $T_{\rm m}$ the lines remain either in a disentangled lattice phase or a metastable state with a frozen degree of entanglement.

IV. DISCUSSION

We have computed the phase diagram of a fluctuating type-II superconductor in the anisotropy-temperature plane. Our results are consistent with general experimental observations that vortex lattice melting occurs well below the crossover $T_{\rm c2}$ associated with the formation of local superconducting order and that the width of this region increases with increasing magnetic field (anisotropy). As was found in earlier isotropic simulations, we continue to find as anisotropy increases that there exists a finite region of the vortex line liquid which possesses superconducting behavior parallel to the applied magnetic field. Such a region has not been seen in other simulations[22] which have used a higher vortex

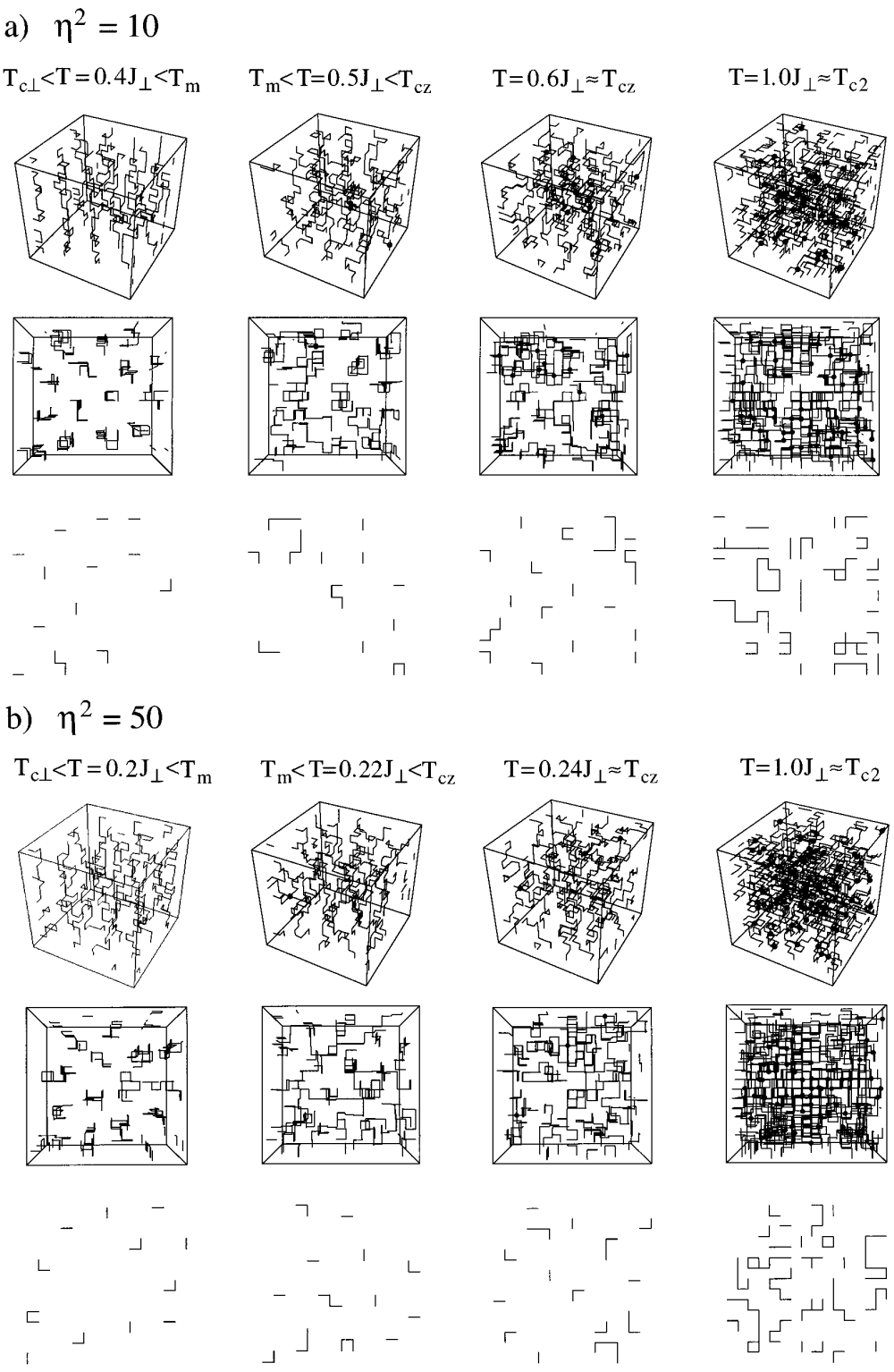

FIG. 16. Snapshot views of vortex line configurations at various temperatures for (a) $\eta^2 = 10$ and (b) $\eta^2 = 50$, for 15^3 size system. For each case we show perspective views from the side (top row) and looking straight down along the applied field (middle row). Solid dots indicate a point of intersection between two vortex line segments. The bottom row is a view of all vortex line segments that lie between a typical pair of adjacent xy planes.

line density $f = 1/5$, 1/6, and 1/8. The transition at T_{cz} from the superconducting line liquid to the normal line liquid appears to be associated with the braiding of a macroscopically large number of field-induced vortex lines, in qualitative agreement with the Nelson-Seung picture based on an analogy with the superfluid transition of two-dimensional bosons.[4] However, unlike the Nelson-Seung picture, T_{cz} does not appear to decrease with increasing L_z. Such a possibility has been proposed by Feigel'man and co-workers[23] in terms of an analogy to 2D bosons with long-range interactions.

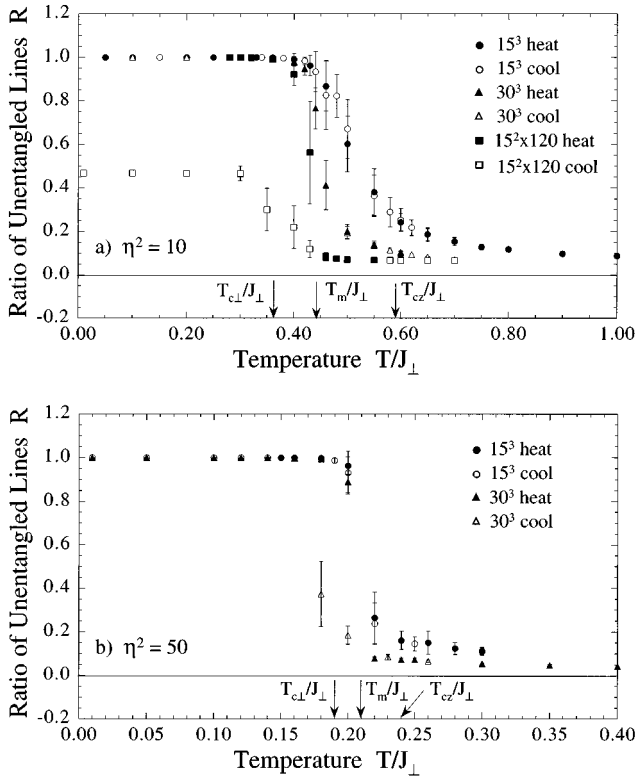

FIG. 17. Fraction of unentangled lines R vs T for various system sizes. (a) is for $\eta^2=10$; (b) is for $\eta^2=50$.

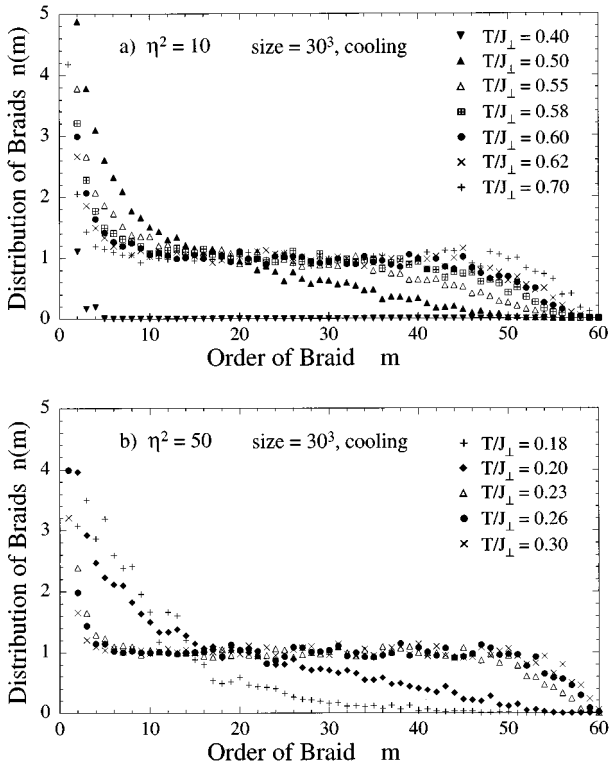

FIG. 18. Braid distribution $n(m)$ vs m for several temperatures near T_{cz}, for system size 30^3. (a) is for $\eta^2=10$; (b) is for $\eta^2=50$.

Recently, Tešanović has proposed[24] a mechanism for such a transition in terms of a vortex loop unbinding analog of the transition at $B=0$. Our numerical results indicate that disconnected thermally induced closed vortex rings do not appear to be playing any significant role at T_{cz}, once the anisotropy has increased enough that T_{cz} is significantly below T_{c2}. However, it remains unclear whether or not vortex rings between planes, which are connected to the field induced lines (see Figs. 15 and 16), are important degrees of freedom.

We have studied behavior as the anisotropy is increased beyond the ''3D-2D'' crossover, which simple dimensional analysis gave as $\eta_{cr}^2 f=1$. We found that this did indeed mark the crossover from η-dependent (3D) behavior to η-independent (2D) behavior, at the high crossover temperature T_{c2}. η_{cr} also corresponds to the region where there is the widest relative width for the floating vortex line lattice, $T_{c\perp}<T<T_m$. However, we see no qualitative changes in critical behavior as η_{cr} is crossed. As η increases above η_{cr}, $T_{c\perp}$, T_m, and T_{cz} all approach each other, but we continue to find $T_{c\perp}\leqslant T_m\leqslant T_{cz}$.

Glazman and Koshelev,[9] by considering the effect of elastic distortions of the vortex line lattice on interplanar phase fluctuations, have argued that T_{cz} should decrease below T_m, with a dependence $T_{cz}\sim\eta^{-1}$, when the anisotropy increases above a value $\sim 10\eta_{cr}$. Frey *et al.*[13] have argued that when $\eta\gg\eta_{cr}$, the proliferation of vortex lattice defects will create a ''supersolid'' phase, leading to $T_{cz}\sim 1/\ln\eta$, which again falls below T_m for large enough η. Similar results were earlier proposed by Feigel'man *et al.*[12] We were unable to equilibrate our system at such high anisotropies so as to more thoroughly check these predictions (very large values of η require relatively large values of $L_\perp$, so that the *total* interplanar coupling energy remains large compared to T). Recently, simulations[16] by Nguyen *et al.*, of a vortex line model with a finite value of $\lambda_\perp<a_v$, find evidence for $T_{cz}<T_m$ for moderate anisotropies. They find $T_{cz}\sim\eta^{-2}$, scaling with the coupling between planes, in contrast to the above two theoretical predictions. They attribute the effect as due to the proliferation of closed vortex rings lying between planes, in contrast with our own findings that such rings do not exist in significant numbers. The point where their T_{cz} crosses below T_m occurs at the value of anisotropy where magnetic coupling between planes starts to dominate over Josephson coupling, $\eta>\lambda_\perp/\xi_\perp$. Their results thus lie outside the range of validity of our infinite $\lambda_\perp$ model [see Eq. (7)]. Simulations by Šášik and Stroud,[25] on an anisotropic

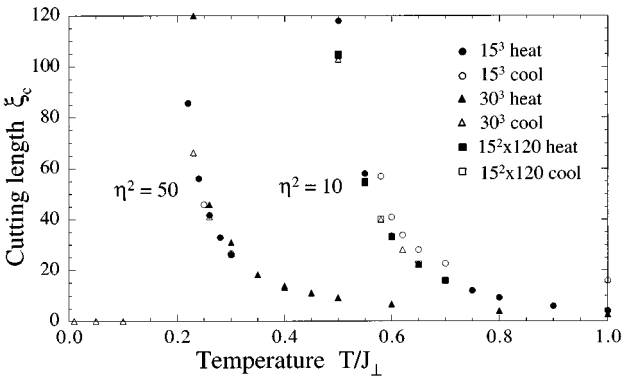

FIG. 19. Cutting length ξ_c vs T for $\eta^2=10$ and 50, for various system sizes.

model in the ''lowest Landau level'' approximation (also a $\lambda_\perp \to \infty$ approximation), always find $T_{cz} = T_m$ for all anisotropies studied. Thus the possibility that parallel coherence can vanish at a *lower* temperature than melting and, if so, the nature of the mechanism responsible remain yet to be clarified numerically.

Finally, we have shown that the effective length over which vortex lines can be considered well-defined connected objects, as measured by the distance between intersections ξ_c, steadily increases once one cools below T_{c2} into the vortex line liquid. This is consistent with the analysis of ''nonlocal'' conductivity in flux transformer experiments, which indicate that correlations parallel to B start to grow right from the onset of strong diamagnetism.[26] Nevertheless, we find that vortex line cutting remains sufficiently easy over most of the vortex line liquid region. This is illustrated by the absence of any hysteresis in the measurement of our entanglement parameter R, for most of the temperature range $T_m < T$ (recall that for our periodic boundary conditions, R can only change value due to the cutting and reconnection of lines). Only for $\eta^2 = 10$ and our thickest $L_z = 120$ did we find freezing into a nonequilibrium state with finite entanglement that sets in near T_m and saturates below $T_{c\perp}$. In earlier isotropic simulations,[8] this freezing out of equilibrium was found to occur at a higher temperature, a little below T_{cz}.

ACKNOWLEDGMENTS

We would like to thank A. E. Koshelev, C. Ciordas-Ciurdariu, and Y.-H. Li, for valuable discussions and assistance. This work has been supported by the U.S. Department of Energy under Grant No. DE-FG02-89ER14017.

[1] M. Tinkham, *Introduction to Superconductivity*, 2nd ed. (McGraw-Hill, New York, 1996).

[2] D. S. Fisher, M. P. A. Fisher, and D. A. Huse, Phys. Rev. B **43**, 130 (1991).

[3] For a recent review see G. Blatter, M. V. Feigel'man, V. B. Geshkenbein, A. I. Larkin, and V. M. Vinokur, Rev. Mod. Phys. **66**, 1125 (1994).

[4] D. R. Nelson and H. S. Seung, Phys. Rev. B **39**, 9153 (1989).

[5] A. Houghton, R. A. Pelcovits, and A. Sudbø, Phys. Rev. B **40**, 6763 (1989); E. H. Brandt, Phys. Rev. Lett. **63**, 1106 (1989).

[6] T. K. Worthington, F. H. Holtzberg, and C. A. Field, Cryogenics **30**, 417 (1990); U. Welp, W. K. Kwok, G. W. Crabtree, K. G. Vandervoort, and J. Z. Liu, Phys. Rev. Lett. **62**, 1908 (1989).

[7] Y.-H. Li and S. Teitel, Phys. Rev. Lett. **66**, 3301 (1991).

[8] Y.-H. Li and S. Teitel, Phys. Rev. B **47**, 359 (1993); **49**, 4136 (1994).

[9] L. I. Glazman and A. E. Koshelev, Phys. Rev. B **43**, 2835 (1991).

[10] D. S. Fisher, in *Phenomenology and Applications of High Temperature Superconductors*, edited by K. Bedell *et al.* (Addison-Wesley, Reading, MA, 1992), p. 287.

[11] For $a_v \gg \xi_\perp$, the interactions between different vortex lines are independent of the core size $\xi_\perp$. However, the self-interaction of a bending vortex line will depend on $\xi_\perp$. This can lead to weak logarithmic dependencies on $\xi_\perp$. See E. H. Brandt, J. Low Temp. Phys. **26**, 735 (1977).

[12] M. V. Feigel'man, V. B. Geshkenbein, and A. I. Larkin, Physica C **167**, 177 (1990).

[13] E. Frey, D. R. Nelson, and D. S. Fisher, Phys. Rev. B **49**, 9723 (1994).

[14] R. Šášik and D. Stroud, Phys. Rev. Lett. **72**, 2462 (1994).

[15] A. E. Koshelev (unpublished).

[16] A. K. Nguyen, A. Sudbø, and R. E. Hetzel, Phys. Rev. Lett. **77**, 1592 (1996).

[17] In 2D, such a floating lattice has been predicted theoretically by D. R. Nelson and B. I. Halperin, Phys. Rev. B **19**, 2457 (1979), and observed in a simulation by M. Franz and S. Teitel, *ibid.* **51**, 6551 (1995) and S. A. Hattel and J. M. Wheatley, *ibid.* **51**, 11 951 (1995). In 3D, the long-range translational order present in a vortex lattice makes it questionable whether, in the presence of a periodic pinning potential, a true floating vortex line lattice phase can ever exist. Nevertheless, if the total pinning energy is small compared to T, a floating lattice may yet exist for 3D simulations of a finite-size system. We thank D. R. Nelson for pointing this out.

[18] For a 2D vortex lattice in a continuum, the melting temperature is at $T_c^{2D} = 0.044 J_\perp$. The rather higher value found here is due to the effects of the discretizing grid. See Franz and Teitel in (Ref. 17).

[19] J. Tobochnik and G. V. Chester, Phys. Rev. B **20**, 3761 (1979).

[20] We refer here to ''geometric'' entanglement as meaning the geometrical twisting of lines around each other. This is in contrast to other, more specific, definitions of entanglement which rigorously relate to the existence of superfluidity in the analog system of 2D bosons (see, for example, Ref.13).

[21] M. C. Marchetti and D. R. Nelson, Phys. Rev. B **42**, 9938 (1990); Physica C **174**, 40 (1991); S. P. Obukhov and M. Rubinstein, Phys. Rev. Lett. **65**, 1279 (1990); **66**, 2279 (1991).

[22] Y.-H. Li and S. Teitel, Phys. Rev. B **45**, 5718 (1992); R. Cavalcanti, G. Carneiro, and A. Gartner, Europhys. Lett. **17**, 449 (1992); G. Carneiro, R. Cavalcanti, and A. Gartner, Phys. Rev. B **47**, 5263 (1993); D. Dominguez, N. Grønbech-Jensen, and A. Bishop, *ibid.* **75**, 4670 (1995); G. Carneiro, *ibid.* **53**, 11 837 (1996); E. A. Jagla and C. A. Balseiro, Phys. Rev. Lett. **77**, 1588 (1996).

[23] M. V. Feigel'man, Physica A **168**, 319 (1990); M. V. Feigel'man, V. B. Geshkenbein, and V. M. Vinokur, JETP Lett. **52**, 546 (1990); M. V. Feigel'man, V. B. Geshkenbein, L. B. Ioffe, and A. I. Larkin, Phys. Rev. B **48**, 16 641 (1993).

[24] Z. Tešanović, Phys. Rev. B **51**, 16 204 (1995).

[25] R. Šášik and D. Stroud, Phys. Rev. B **52**, 3696 (1995).

[26] H. Safar, P. L. Gammel, D. A. Huse, S. N. Majumdar, L. F. Schneemeyer, D. J. Bishop, D. López, G. Nieva, and F. de la Cruz, Phys. Rev. Lett. **72**, 1272 (1994).